Phase transitions in pyrolitic mantle around 670-km depth: Implications for upwelling of plumes from the lower mantle

Kei Hirose

Department of Earth and Planetary Sciences, Tokyo Institute of Technology, Tokyo, Japan

Received 27 April 2001; revised 14 September 2001; accepted 23 September 2001; published 26 April 2002.

[1] Phase relations in the natural pyrolitic mantle composition (KLB-1) around 670-km depth have been determined at 1600–2200°C by high-pressure experiments using multianvil apparatus. A phase transition between majorite garnet and Al-bearing Mg-rich perovskite occurs at depths similar to the postspinel phase transition. The seismic discontinuity observed at this depth could be caused by a combination of both transitions. The majorite-perovskite transition boundary has a positive Clausius-Clapeyron slope (+0.0013 GPa/°C for majorite-out curve), in contrast to the negative slope of the postspinel phase boundary (−0.0028 GPa/°C). Both transition boundaries cross each other at 1700–1800°C. Below this temperature, formation of Mg-perovskite starts at the majorite-perovskite or akimotoite-perovskite transition coexisting with ringwoodite but is predominantly formed by the postspinel phase transition at higher pressures. On the other hand, the stability of majorite significantly expands relative to Mg-perovskite at higher temperatures. Majorite becomes a dominant postspinel phase, and a majority of Mg-perovskite is formed by the majorite-perovskite transition with a positive Clapeyron slope. Phase transition within high-temperature plumes (>1800°C at 670-km depth) assists their upwelling from the lower mantle through the 670-km boundary. The depth of the 670-km seismic discontinuity becomes much less temperature-sensitive and is greater in such a higher temperature region. *INDEX TERMS:* 3630 Mineralogy and Petrology: Experimental mineralogy and petrology; 3924 Mineral Physics: High-pressure behavior; 8424 Volcanology: Hydrothermal systems (8135); *KEYWORDS:* Pyrolite, 670-km depth, plume, phase transition, lower mantle

1. Introduction

[2] The 670-km depth seismic discontinuity is marked by the formation of perovskite, which is much denser than the upper mantle minerals (~10%). It has long been believed to be a barrier for mantle convection, impeding subduction of slabs or upwelling of hot plumes, because the postspinel phase boundary has a negative Clausius-Clapeyron slope [*Ito and Takahashi*, 1989; *Akaogi and Ito*, 1993]. *P* wave tomographic images have revealed stagnant slabs around 670-km depth in many subduction zones before they sink to the bottom of the mantle [e.g., *Van der Hilst et al.*, 1991; *Fukao et al.*, 1992]. On the other hand, plumes, many of which may originate from the lower mantle, are not found to be stagnant around this depth. This implies that the style of vertical movement through the 670-km depth boundary may be different at high temperatures.

[3] Phase relations of pyrolitic mantle around 670-km depth are rather complicated because the postspinel phase transition and the majorite garnet to Al-bearing $MgSiO_3$-rich perovskite transition occur at similar depths. As seen in Figure 1, majorite-perovskite transition pressures are strongly dependent on chemical composition especially Al_2O_3, contrary to the postspinel phase transition. The transition pressure becomes higher with increasing Al_2O_3 content; 22.4 GPa in $MgSiO_3$ [*Hirose et al.*, 2001b], 22.7–23.8 GPa in pyrolite (4% Al_2O_3) (this study), 26.0–26.7 GPa in basalt (15% Al_2O_3) [*Hirose et al.*, 1999], and 27.3 GPa in $Mg_3Al_2Si_3O_{12}$ ($MgSiO_3$ + 25% Al_2O_3) [*Hirose et al.*, 2001a] at 1800°C. The majorite-perovskite transition boundary has a positive pressure-temperature slope in contrast to the negative slope of the postspinel phase boundary. Phase transition pressures therefore are strongly dependent on temperature.

0148-0227/02/2001JB000597$09.00

[4] In this study, phase relations of pyrolitic mantle (KLB-1) were determined in a wide temperature range (1600–2200°C). The stabilities of majorite and Mg-perovskite are strongly dependent on temperature as well as chemical composition [e.g., *Irifune et al.*, 1996; *Hirose et al.*, 2001a]. The temperature effect, however, has not been studied in previous studies (1500°C [*Irifune*, 1994] and 1627°C [*Wood*, 2000]). Majorite has a wide stability relative to Mg-perovskite and plays an important function in dynamics at high temperatures. This has been discussed by *Weidner and Wang* [1998] in the simplified system, using the limited experimental data available at that time. In this paper, the role of the Mg-perovskite to majorite transition in the penetration of hot plumes through the 670-km boundary is discussed, using new experimental results on the natural composition.

2. Experiments

2.1. Pressure Calibration

[5] The pressure calibration in the multianvil apparatus is the focus of debate at present [*Irifune et al.*, 1998; *Hirose et al.*, 2001a]. Pressure above 20 GPa has been calibrated using akimotoite (ilmenite)-perovskite transition pressure in $MgSiO_3$ in all the high-pressure laboratories, which was determined by conventional quench experiments [*Ito and Takahashi*, 1989]. However, the recent in situ X-ray diffraction measurements at synchrotron radiation source showed that the phase transition boundaries in $MgSiO_3$ [*Kuroda et al.*, 2000; *Ono et al.*, 2001; *Hirose et al.*, 2001b], Mg_2SiO_4 [*Irifune et al.*, 1998], and $Mg_3Al_2Si_3O_{12}$ [*Hirose et al.*, 2001a], based on the gold pressure scale proposed by *Anderson et al.* [1989], are consistently lower by 2 GPa than those determined by quench experiments.

[6] However, the results of in situ measurements depend largely on the choice of pressure standard and *P-V-T* equation of state.

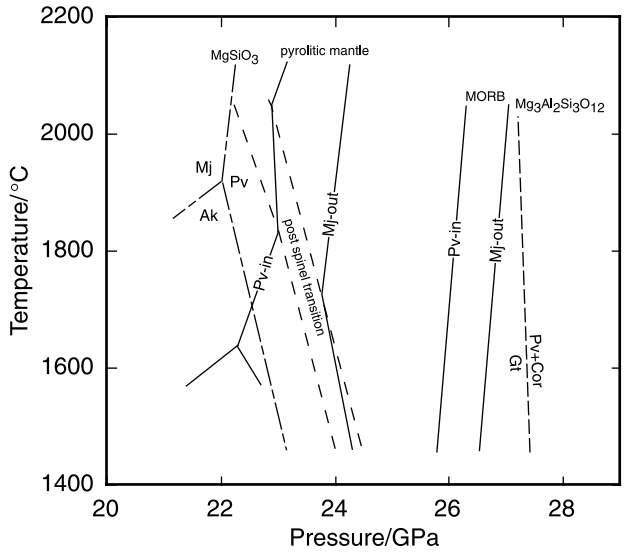

Figure 1. Majorite-perovskite transitions in different bulk compositions; majorite-perovskite transition in $MgSiO_3$ [*Hirose et al.*, 2001b], Mg-perovskite-in and majorite-out curves in pyrolite (this study) and mid-ocean ridge basalt (MORB) [*Hirose et al.*, 1999], and garnet-perovskite plus corundum transition in $Mg_3Al_2Si_3O_{12}$ [*Hirose et al.*, 2001a]. The dashed lines indicate the postspinel phase boundary in pyrolite. Note that majorite-perovskite transition pressures are strongly dependent on the chemical composition, contrary to the postspinel phase boundary.

Both in situ and quench results on ilmenite-perovskite transition in $MgSiO_3$ are perfectly consistent [*Ono et al.*, 2001; *Hirose et al.*, 2001b] if another equation of state of gold proposed by *Jamieson et al.* [1982] is applied to the in situ data instead of *Anderson et al.*'s [1989] equation.

[7] In the present quench experiments, gold pressure scale proposed by *Jamieson et al.* [1982] was primarily used (Table 1). Pressures driven by the multianvil press at the Tokyo Institute of Technology were calibrated at 1750°C, with reference to the transition pressures determined by in situ measurements using Jamieson et al.'s equation of state of gold; akimotoite (ilmenite)-perovskite transition in $MgSiO_3$ at 22.4 GPa [*Ono et al.*, 2001; *Hirose et al.*, 2001b] and garnet-perovskite + corundum transition in $Mg_3Al_2Si_3O_{12}$ at 27.2 GPa [*Hirose et al.*, 2001a]. The present pressure calibration is consistent with our previous one using *Ito and Takahashi*'s [1989] ilmenite-perovskite transition pressure in $MgSiO_3$. Experimental pressures calibrated on the basis of *Anderson et al.*'s [1989] gold scale are also shown in Table 1.

[8] The postgarnet phase boundary in $Mg_3Al_2Si_3O_{12}$ is proposed as a new high-pressure calibration point for quench experiments to establish a consistent pressure scale at high temperatures. Pressure scales for the quench experiments above 23 GPa have been inconsistent between laboratories as much as 2 GPa [*Hirose et al.*, 1999] because pressure was not calibrated above the ilmenite-perovskite transition in $MgSiO_3$.

[9] The temperature effect on pressure calibration was estimated by in situ measurements at SPring-8, according to two calibration runs at the fixed load force of the apparatus (Figure 2). Pressure dropped from 26.1 GPa at 500°C to 24.6 GPa at 2000°C, based on the *Jamieson et al.*'s [1982] gold scale. The same high-pressure assembly and gasket were used for the quench experiments in this study. A phase transition boundary in $Mg_3Al_2Si_3O_{12}$ determined by in situ measurements was well reconstructed by the quench experiments using the present estimate of temperature effect [*Hirose et al.*, 2001a]. The reproducibility of pressure in the present quench experiments was less than ±0.2 GPa, based on the force load-pressure relation in in situ measurements [*Hirose et al.*, 2001b].

2.2. Experiments

[10] High-pressure experiments were made under dry conditions at 22–25 GPa and 1600–2200°C. The 8/3 assembly (8-mm octahedron edge length and 3-mm truncated edge length of tungsten carbide), the same as described by *Bertka and Fei* [1997], was

Table 1. Experimental Conditions and Run Products[a]

Run	Pressure,[b] GPa		*T*, °C	*t*, min	Run Products[c]
	Anderson	Jamieson			
⟨Mg_2SiO_4⟩					
C114	20.8	23	2000	17	Wd
C118	21.25	23.45	2000	30	Pv + Pe
C117	22	24.3	2000	24	Pv + Pe
C119	20.9	23.1	1800	60	Wd
C122	21.35	23.5	1800	60	Rw
C121	21.75	24.05	1800	60	Pv + Pe
⟨KLB-1⟩					
C110	20.8	23	2200	10	Mj(78) + Mw(19) + Ca-pv(3)
C132	20.8	23	2000	60	Rw(31) + Mj(57) + Mw(10) + Ca-pv(2)
C133	21.25	23.45	2000	60	Mj(24) + Mg-pv(54) + Mw(17) + Ca-pv(5)
C173	22	24.3	2000	30	Mg-pv(77) + Mw(17) + Ca-pv(6)
C188	20.45	22.6	1800	150	Rw(62) + Mj(34) + Ca-pv(4)
C186	20.9	23.1	1800	120	Rw(35) + Mj(16) + Mg-pv(36) + Mw(9) + Ca-pv(4)
C185	21.4	23.7	1800	120	Mj(7) + Mg-pv(72) + Mw(15) + Ca-pv(6)
C176	21.75	24.05	1800	120	Mg-pv(78) + Mw(16) + Ca-pv(6)
C134	22.5	24.9	1800	180	Mg-pv(79) + Mw(15) + Ca-pv(6)
C190	20	22	1600	485	Rw(65) + Mj(28) + Ak(2) + Ca-pv(5) + St(trace)
C189	20.55	22.6	1600	404	Rw(59) + Mj(19) + Mg-pv(17) + Ca-pv(5)
C179	21.45	23.6	1600	180	Rw(63) + Mj(16) + Mg-pv(16) + Ca-pv(5)
C187	21.85	24.05	1600	480	Rw(28) + Mg-pv(60) + Mw(6) + Ca-pv(6)
C182	22.3	24.55	1600	190	Mg-pv(78) + Mw(15) + Ca-pv(7)

[a] Wd, wadslyite; Rw, ringwoodite; Mj, majorite garnet; Ak, akimotoite; Pv or Mg-pv, Mg-rich perovskite; Pe, periclase; Mw, magnesiowustite; St, stishovite; Ca-pv, Ca-rich perovskite.
[b] Pressures were calibrated on the basis of equation of state of gold proposed by *Anderson et al.* [1989] and *Jamieson et al.* [1982].
[c] Numbers in parentheses indicate weight fraction of each phase.

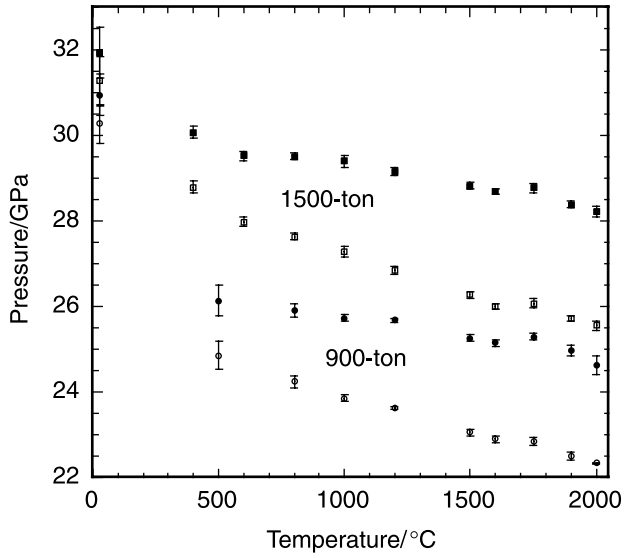

Figure 2. Temperature effect on pressure generation at the fixed load force of the apparatus, at 900 (circles) and 1500 t (squares). Pressures were calculated using both the equations of state of gold proposed by *Jamieson et al.* [1982] (solid symbols) and *Anderson et al.* [1989] (open symbols). The choice of equation of state gives ~2 GPa difference using the same X-ray diffraction data.

used for multianvil apparatus (MA6-8). Experiments were done both on Mg_2SiO_4 forsterite and natural peridotite KLB-1 (Table 1). For the peridotite starting materials, both synthesized gel and natural rock fine powder were prepared. The peridotite KLB-1 is similar in composition to pyrolite and has been used in many high-pressure studies [e.g., *Takahashi*, 1986; *Hirose and Kushiro*, 1993; *Zhang and Herzberg*, 1994; *Kawamoto and Holloway*, 1997]. The starting materials were loaded into a Re capsule. Temperature was monitored with W5Re-W26Re thermocouple. The experimental conditions and phase assemblages are summarized in Table 1. Phase identification was made by a combination of microfocused (50–100 μm) X-ray diffraction technique (RIGAKU RINT-2500), micro-Raman spectroscopy, and microprobe.

[11] The chemical compositions of coexisting phases were obtained by the microprobe analyses, which are summarized in Table 2. The grain sizes of the run products synthesized from the gel starting material were smaller than those from the rock powder and were often too small to have analyses. The results therefore include analyses on the run products from both the starting materials. Analyses were made very carefully especially for majorite and perovskite; they were obtained only on the coexisting grains next to each other because the run products from the rock powder were very heterogeneous in Al_2O_3 as was discussed by *Wood* [2000]. Even in the run products synthesized from the rock powder, the grain sizes of Ca-perovskite and magnesiowüstite were too small for electron microprobe analysis in many of the experiments, especially at 1600°C.

3. Results

3.1. Postspinel Phase Transition Boundary

[12] It is widely believed that the seismic discontinuity at 670-km depth is caused by the postspinel phase transition. This idea was supported also by the high-pressure experiments applying quench method [*Ito and Takahashi*, 1989]. However, the first in situ measurements of this phase transition by *Irifune et al.* [1998] showed that the transition pressure is 2 GPa lower than the previous estimates, suggesting that the postspinel phase transition pressure does not match with the depth of the 670-km discontinuity.

[13] The postspinel transition boundary was further examined by applying another pressure scale and by conducting diamond cell experiments. The results of in situ measurements depend on the choice of pressure standard and *P-V-T* equation of state by which pressure is calculated [*Hirose et al.*, 2001a, 2001b; *Ono et al.*, 2001]. *Hirose et al.* [2001a] pointed out that the transition pressure determined by *Irifune et al.* [1998] coincides with 670-km depth, if *Jamieson et al.*'s [1982] equation of state of gold is applied to their in situ data instead of *Anderson et al.*'s [1989] equation. The recent laser-heated diamond cell experiments also showed that the postspinel phase transition pressure matches with 670-km depth both by platinum pressure scale [*Shim et al.*, 2001] and by ruby scale [*Chudinovskikh and Boehler*, 2001]. At this point, however, the exact pressure of postspinel phase transition boundary is still controversial because (1) the accuracy of these pressure scales is not clear and (2) the pressure effect on emf of the thermocouple is uncertain.

[14] The postspinel phase transition pressure in Mg_2SiO_4 determined in this study using *Jamieson et al.*'s [1982] gold scale matches with the depth of the 670-km discontinuity (Figure 3). On the other hand, if *Anderson et al.*'s [1989] gold scale is applied to the experiments same as *Irifune et al.* [1998], the transition pressure shifts 2 GPa lower than that based on the Jamieson et al.'s scale, corresponding to a depth of 610 km and is closely consistent with their in situ measurements.

[15] The postspinel phase transition boundary in the natural pyrolitic mantle composition (KLB-1) is compared in Figure 3. The boundary has some pressure interval in the natural composition containing Al_2O_3. The ringwoodite-out curve is very close to the boundary in Mg_2SiO_4. The stability of ringwoodite is limited in Mg_2SiO_4 at high temperatures, and wadslyite directly decomposes to perovskite and periclase at 2000°C [*Kuroda et al.*, 2000].

3.2. Phase Relations of Pyrolitic Mantle

[16] The phase relations of natural pyrolitic mantle composition are shown in Figure 4. The mineral assemblages of the run products synthesized from gel and natural rock powder were sometimes different as seen from the X-ray diffraction data. For example, in the run product C176, majorite was included in the latter but not in the former. Microprobe observation showed a heterogeneous distribution especially of Al_2O_3 in the sample synthesized from the rock powder because aluminous spinel did not fully react with other high-pressure phases. An Al-rich silicate phase was often observed in these run products. On the other hand, the gel is quite homogeneous in composition and rapidly reaches near-equilibrium at high pressure and temperature [e.g., *Ono and Yasuda*, 1996]. The mineral assemblage synthesized from gel starting material is therefore believed to represent the equilibrium assemblage. Moreover, the stabilities of majorite and perovskite in the run products from gel are consistent with the Al_2O_3 contents in these minerals.

[17] The results are generally consistent with the phase transitions in the simple system of Mg_2SiO_4, $MgSiO_3$, and on the join $MgSiO_3$-$Mg_3Al_2Si_3O_{12}$. The stability of akimotoite in the natural pyrolite composition was recognized in a small pressure interval around 22 GPa at 1600°C in this study. It was clearly identified by Raman spectroscopy and microprobe analysis. The stability of akimotoite is limited to low-temperature conditions in the Fe-bearing system, although it is stable in a wide pressure and temperature range up to 1920°C in $MgSiO_3$ composition [*Hirose et al.*, 2001b]. Akimotoite was not observed above 1600°C in the natural pyrolitic composition. A trace amount of stishovite was also found at 22 GPa and 1600°C, consistent with the observation that ringwoodite and stishovite coexist in $MgSiO_3$ composition [*Sawamoto*, 1987].

Table 2. Chemical Compositions of Coexisting Minerals[a]

	SiO_2	TiO_2	Al_2O_3	FeO	MgO	CaO	Na_2O	K_2O	Cr_2O_3	Total
C110										
Mj	55.70(0.41)	0.06(0.01)	4.65(0.56)	4.56(0.26)	32.10(0.65)	2.63(0.31)	0.17(0.06)	0.01(0.01)	0.46(0.08)	100.32
Mw	0.26(0.21)	0.02(0.02)	0.47(0.08)	21.39(0.04)	76.67(0.44)	0.06(0.03)	0.27(0.04)	0.01(0.01)	0.47(0.00)	99.63
Ca-pv	44.72	1.06	2.25	0.73	1.13	41.67	0.32	0.08	0.05	91.99
C132										
Rw	41.38(0.29)	0.03(0.01)	0.14(0.03)	10.45(0.31)	48.79(0.44)	0.10(0.05)	0.13(0.01)	0.02(0.01)	0.10(0.02)	101.14
Mj	54.50(0.63)	0.14(0.02)	5.70(1.14)	5.39(0.54)	30.17(1.03)	4.34(0.69)	0.30(0.10)	0.01(0.01)	0.48(0.17)	101.03
Mw	0.44(0.33)	0.02(0.02)	0.30(0.02)	24.51(0.96)	73.44(1.16)	0.09(0.04)	0.45(0.04)	0.02(0.01)	0.40(0.03)	99.67
Ca-pv[b]	44.02	1.44	2.04	1.34	4.32	37.05	0.53	0.14	0.17	91.05
C133										
Mj	53.64(0.51)	0.03(0.02)	6.48(0.44)	4.84(0.13)	30.66(0.65)	3.11(0.36)	0.48(0.05)	0.01(0.01)	0.47(0.07)	99.72
Mg-pv	55.74(1.13)	0.13(0.04)	3.61(0.58)	5.85(0.73)	36.59(0.50)	0.70(0.18)	0.09(0.03)	0.01(0.01)	0.23(0.04)	102.94
Mw	0.59	0.00	0.05	22.46	73.02	0.00	0.44	0.00	0.45	97.02
C173										
Mg-pv	54.44(1.34)	0.11(0.04)	4.83(0.22)	6.83(0.31)	33.58(0.73)	0.68(0.25)	0.10(0.02)	0.01(0.01)	0.31(0.05)	100.87
C188										
Rw	41.22(0.59)	0.06(0.02)	0.41(0.29)	9.70(0.19)	48.57(1.13)	0.47(0.28)	0.13(0.05)	0.02(0.01)	0.09(0.02)	100.68
Mj	50.78(1.10)	0.03(0.02)	10.57(1.97)	4.97(0.34)	27.99(0.70)	4.57(0.45)	0.27(0.04)	0.02(0.01)	0.70(0.12)	99.89
Ca-pv	42.52(0.38)	3.03(0.07)	1.91(0.06)	1.17(0.03)	1.15(0.11)	43.64(1.01)	0.32(0.08)	0.05(0.02)	0.14(0.02)	93.94
C186										
Rw	40.61(0.24)	0.06(0.01)	0.21(0.02)	9.82(0.16)	48.87(0.11)	0.38(0.12)	0.08(0.01)	0.02(0.02)	0.07(0.00)	100.13
Mj	51.41(1.67)	0.03(0.03)	10.15(2.15)	4.61(0.26)	27.79(1.27)	4.59(0.64)	0.44(0.08)	0.01(0.01)	0.68(0.07)	99.71
Mg-pv	56.21(0.51)	0.32(0.09)	3.97(0.26)	4.89(0.32)	36.55(0.72)	0.22(0.13)	0.06(0.06)	0.01(0.02)	0.31(0.03)	102.54
Mw	0.71(0.78)	0.02(0.01)	0.23(0.03)	24.13(0.64)	74.98(0.22)	0.06(0.05)	0.61(0.05)	0.01(0.01)	0.33(0.03)	101.08
C185										
Mj	49.86(1.04)	0.03(0.02)	12.39(0.83)	4.28(0.07)	28.53(0.34)	4.42(0.34)	0.39(0.06)	0.01(0.01)	0.77(0.03)	100.68
Mg-pv	55.83(0.66)	0.22(0.10)	3.85(0.21)	5.60(0.34)	37.55(0.61)	0.55(0.51)	0.06(0.02)	0.01(0.01)	0.31(0.03)	103.97
Mw	0.64(0.30)	0.01(0.01)	0.30(0.08)	22.18(0.28)	76.66(0.57)	0.28(0.24)	0.59(0.06)	0.02(0.01)	0.46(0.04)	101.13
C176										
Mg-pv	54.90(0.87)	0.23(0.10)	4.94(0.43)	6.92(0.37)	35.98(1.19)	0.37(0.35)	0.10(0.04)	0.02(0.02)	0.36(0.08)	103.81
Ca-pv	49.03	0.57	1.58	0.95	1.84	47.14	0.18	0.06	0.08	101.43
C134										
Mg-pv	53.03(0.56)	0.15(0.03)	5.17(0.25)	6.56(0.15)	35.32(0.70)	0.79(0.08)	0.10(0.04)	0.00(0.00)	0.30(0.02)	101.42
C190										
Rw	41.56(0.29)	0.06(0.02)	0.33(0.51)	10.36(0.27)	47.19(0.67)	0.23(0.29)	0.06(0.02)	0.01(0.01)	0.08(0.04)	99.87
Mj	50.73(2.25)	0.06(0.03)	11.42(2.71)	5.20(0.36)	28.29(1.46)	3.69(0.76)	0.26(0.04)	0.01(0.01)	0.94(0.22)	100.60
Ak	58.67	0.25	0.60	2.83	37.89	0.17	0.04	0.02	0.09	100.56
St	93.88	0.06	0.32	0.62	1.96	0.35	0.01	0.02	0.01	97.21
Ca-pv[b]	47.87	2.61	1.17	0.84	2.84	41.12	0.15	0.02	0.12	96.75
C189										
Rw	40.87(0.75)	0.02(0.02)	0.31(0.30)	10.74(0.17)	47.91(0.78)	0.22(0.19)	0.15(0.05)	0.02(0.02)	0.16(0.03)	100.39
Mj	47.92(1.02)	0.05(0.03)	13.95(1.91)	5.48(0.25)	24.68(1.34)	5.05(0.70)	0.81(0.20)	0.04(0.03)	1.26(0.14)	99.24
Mg-pv	55.82(1.30)	0.14(0.03)	3.88(0.51)	6.61(0.55)	36.61(1.29)	0.22(0.11)	0.07(0.06)	0.02(0.02)	0.33(0.03)	103.71
C179										
Rw	41.40(0.34)	0.02(0.03)	0.09(0.08)	11.14(0.04)	47.51(0.46)	0.05(0.04)	0.07(0.03)	0.01(0.01)	0.08(0.04)	100.36
Mj	46.65(0.94)	0.01(0.01)	16.45(2.08)	5.06(0.55)	25.28(2.13)	3.90(0.66)	0.44(0.07)	0.03(0.02)	1.57(0.18)	99.39
Mg-pv	56.92(0.51)	0.10(0.03)	4.20(0.31)	6.02(0.38)	35.32(1.07)	0.71(0.21)	0.13(0.04)	0.02(0.01)	0.27(0.03)	103.69
C187										
Rw	40.71(1.25)	0.01(0.01)	0.12(0.02)	9.32(0.15)	49.58(0.60)	0.04(0.02)	0.13(0.03)	0.02(0.01)	0.07(0.03)	99.99
Mg-pv	52.93(0.36)	0.25(0.08)	5.13(0.24)	7.72(0.27)	36.43(0.72)	0.60(0.30)	0.10(0.03)	0.02(0.01)	0.34(0.02)	103.50
C182										
Mg-pv	54.53(1.43)	0.48(0.27)	4.94(0.42)	6.63(0.88)	36.45(0.59)	0.27(0.13)	0.19(0.06)	0.02(0.01)	0.32(0.03)	103.83

Table 2. (continued)

	Si	Ti	Al	Fe	Mg	Ca	Na	K	Cr	Total (O = 24)
C110										
Mj	7.64	0.01	0.75	0.52	6.56	0.39	0.05	0.00	0.05	15.98
Mw	0.05	0.00	0.10	3.17	20.27	0.01	0.09	0.00	0.07	23.92
Ca-pv	7.52	0.09	0.45	0.16	0.42	7.42	0.10	0.02	0.02	16.21
C132										
Rw	6.02	0.00	0.02	1.27	10.58	0.02	0.04	0.00	0.01	17.98
Mj	7.50	0.01	0.93	0.62	6.19	0.64	0.08	0.00	0.05	16.04
Mw	0.08	0.00	0.06	3.69	19.72	0.02	0.16	0.00	0.06	23.94
Ca-pv[b]										
C133										
Mj	7.44	0.00	1.06	0.56	6.34	0.46	0.13	0.00	0.05	16.07
Mg-pv	7.48	0.01	0.57	0.66	7.32	0.10	0.02	0.00	0.02	16.22
Mw	0.11	0.00	0.01	3.45	19.97	0.00	0.16	0.00	0.06	23.93
C173										
Mg-pv	7.48	0.01	0.78	0.78	6.88	0.10	0.03	0.00	0.03	16.11
C188										
Rw	6.01	0.01	0.07	1.18	10.56	0.07	0.04	0.00	0.01	17.96
Mj	7.08	0.00	1.74	0.58	5.82	0.68	0.07	0.00	0.08	16.05
Ca-pv	7.14	0.38	0.38	0.16	0.29	7.85	0.10	0.01	0.02	16.34
C186										
Rw	5.97	0.01	0.04	1.21	10.71	0.06	0.02	0.00	0.01	18.02
Mj	7.16	0.00	1.67	0.54	5.77	0.69	0.12	0.00	0.08	16.02
Mg-pv	7.53	0.03	0.63	0.55	7.30	0.03	0.01	0.00	0.03	16.12
Mw	0.13	0.00	0.05	3.59	19.89	0.01	0.21	0.00	0.05	23.93
C185										
Mj	6.88	0.00	2.02	0.49	5.87	0.65	0.10	0.00	0.08	16.12
Mg-pv	7.42	0.02	0.60	0.62	7.44	0.08	0.01	0.00	0.03	16.24
Mw	0.11	0.00	0.06	3.27	20.16	0.05	0.20	0.00	0.06	23.93
C176										
Mg-pv	7.35	0.02	0.78	0.77	7.18	0.05	0.03	0.00	0.04	16.23
Ca-pv	7.54	0.07	0.29	0.12	0.42	7.77	0.05	0.01	0.01	16.28
C134										
Mg-pv	7.28	0.02	0.84	0.75	7.22	0.12	0.03	0.00	0.03	16.29
C190										
Rw	6.10	0.01	0.06	1.27	10.33	0.04	0.02	0.00	0.01	17.87
Mj	7.01	0.01	1.86	0.60	5.83	0.55	0.07	0.00	0.10	16.03
Ak	7.91	0.03	0.10	0.32	7.62	0.02	0.01	0.00	0.01	16.02
St	11.72	0.01	0.05	0.06	0.36	0.05	0.00	0.00	0.00	12.25
Ca-pv[b]										
C189										
Rw	6.01	0.00	0.05	1.32	10.50	0.03	0.04	0.00	0.02	17.98
Mj	6.78	0.01	2.33	0.65	5.20	0.77	0.22	0.01	0.14	16.10
Mg-pv	7.46	0.01	0.61	0.74	7.30	0.03	0.02	0.00	0.04	16.21
C179										
Rw	6.08	0.00	0.02	1.37	10.40	0.01	0.02	0.00	0.01	17.92
Mj	6.55	0.00	2.72	0.59	5.29	0.59	0.12	0.00	0.17	16.06
Mg-pv	7.58	0.01	0.66	0.67	7.01	0.10	0.03	0.00	0.03	16.09
C187										
Rw	5.97	0.00	0.02	1.14	10.84	0.01	0.04	0.00	0.01	18.03
Mg-pv	7.17	0.03	0.82	0.87	7.35	0.09	0.03	0.00	0.04	16.39
C182										
Mg-pv	7.30	0.05	0.78	0.74	7.27	0.04	0.05	0.00	0.03	16.27

[a] Rw, ringwoodite; Mj, majorite garnet; Ak, akimotoite; Mg-pv, Mg-rich perovskite; Mw, magnesiowustite; St, stishovite; Ca-pv, Ca-rich perovskite. Numbers in parentheses indicate one standard deviation in the analyses.

[b] Electron beam may have overlapped with adjacent minerals.

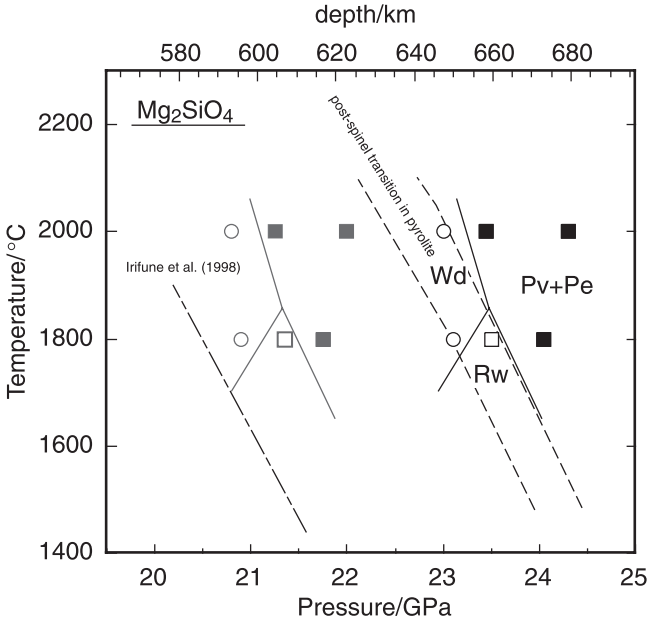

Figure 3. Phase boundaries in Mg_2SiO_4 determined in this study. The solid and shaded symbols are based on the *Jamieson et al.*'s [1982] and *Anderson et al.*'s [1989] gold pressure scales, respectively. The postspinel phase transition pressure based on the Jamieson et al.'s scale matches with the depth of the 670-km seismic discontinuity. The dashed lines indicate the postspinel phase boundary in pyrolite from Figure 4.

[18] The phase relations of natural pyrolite composition are very sensitive to the temperature and rather complicated at 22–24 GPa. This is because (1) the postspinel transition and the majorite-perovskite transition occur at similar pressures and (2) these transition boundaries have negative and positive Clausius-Clapeyron slopes, respectively. The postspinel phase transition occurs in a pressure range from 23.6 to 24.1 GPa at 1600°C with a negative Clapeyron slope (−0.0028 GPa/°C). This pressure range corresponds to the depth of the 670-km seismic discontinuity. The transition between majorite and Al-bearing Mg-rich perovskite occurs in a wider pressure interval of 1–1.5 GPa. The Clapeyron slope was not well constrained by the present study but is +0.0013 GPa/°C for the majorite-out curve. The Mg-perovskite-in curve is more temperature-dependent. Both transition boundaries cross each other approximately at 1700–1800°C. The majorite-perovskite transition occurs at pressures higher than the postspinel phase boundary above 1800°C, while it occurs also in the presence of ringwoodite below 1800°C. The temperature has thus significant effects on the phase relations.

[19] It has been believed that Mg-rich perovskite primarily forms by the postspinel phase transition with a negative Clapeyron slope. The present study, however, demonstrates that the formation of Mg-perovskite occurs by various reactions; akimotoite-perovskite, majorite-perovskite, and postspinel phase transition shown in Figure 4. The pressure of Mg-perovskite formation strongly depends on temperature. Below 1700–1800°C, the contours of volume fraction of Mg-perovskite in the bulk pyrolite (0, 25, 50, and 78%) have negative pressure-temperature slopes, indicating that it is primarily formed by the decomposition of ringwoodite. On the other hand, they have a temperature-independent or positive pressure-temperature slopes above 1700–1800°C. It indicates that they are formed rather by majorite-perovskite phase transition at high temperatures.

[20] At 1600°C the Mg-perovskite-in curve corresponds to the akimotoite-perovskite transition boundary. Mg-perovskite is stable coexisting with ringwoodite in a wide pressure range from 22.5 to 24.1 GPa. Majorite disappears when half of ringwoodite decomposes. At 1800°C the formation of Mg-perovskite commences at the majorite-perovskite transition. Both the postspinel phase and the majorite-perovskite transitions occur in a narrow pressure

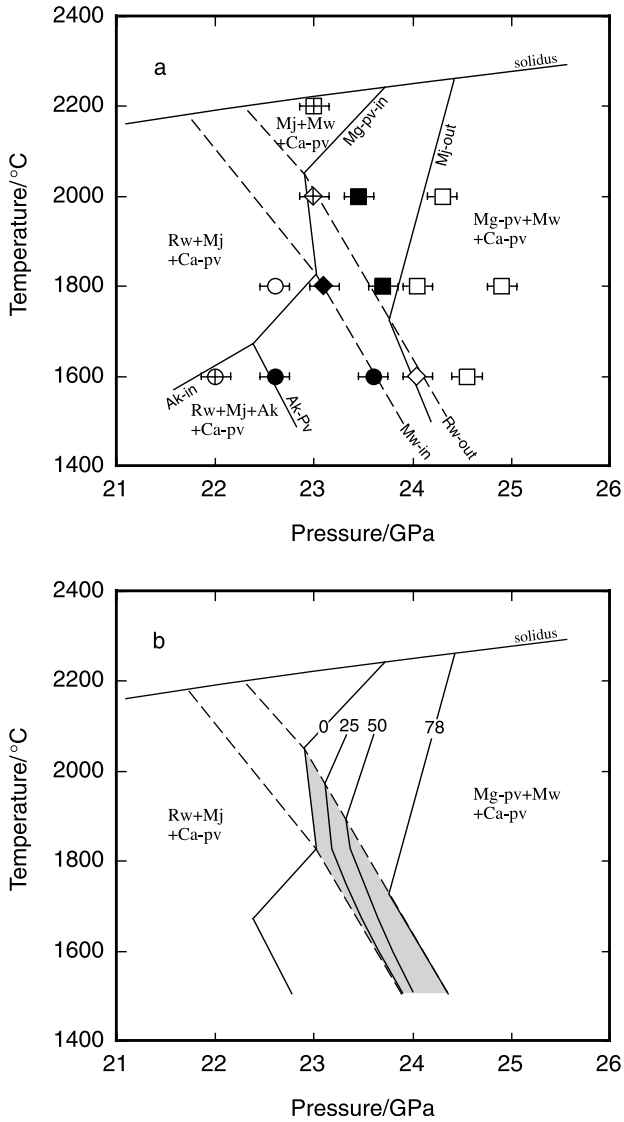

Figure 4. Phase relations in the pyrolitic mantle composition (KLB-1). Solidus curve is from *Herzberg et al.* [2000]. (a) The error bars indicate the reproducibility of pressure in the quench experiments. The solid symbols indicate coexisting assemblages of majorite (Mj) and Mg-perovskite (Mg-pv). Open circle, ringwoodite (Rw) + Mj + Ca-perovskite (Ca-pv); circle with cross, Rw + Mj + akimotoite (Ak) + Ca-pv; solid circle, Rw + Mj + Mg-pv + Ca-pv; open square, Mg-pv + magnesiowüstite (Mw) + Ca-pv; square with cross, Mj + Mw + Ca-pv; solid square, Mj + Mg-pv + Mw + Ca-pv; open diamond, Rw + Mg-pv + Mw + Ca-pv; diamond with cross, Rw + Mj + Mw + Ca-pv; solid diamond, Rw + Mj + Mg-pv + Mw + Ca-pv. (b) The transformation to Mg-perovskite occurs in a wide pressure range. The volume fraction of Mg-perovskite is shown by contours. The 25, 50, and 78% contours have temperature-independent or positive pressure-temperature slopes above 1700–1800°C. The shaded area shows the conditions in which Mg-perovskite is formed by the postspinel phase transition. Note that the more Mg-perovskite is formed by the majorite-perovskite transition rather than the postspinel phase transition at higher temperatures.

range. At 2000°C, ringwoodite decomposes primarily into majorite and magnesiowüstite. Mg-perovskite is formed when ~70% of ringwoodite decomposes. Majorite was the predominant mineral in the run product C132. It has a wide stability at pressures higher than the postspinel phase boundary at 2000°C. At higher temperatures such as 2200°C, ringwoodite decomposes only into majorite and magnesiowüstite in the presence of trace Ca-rich perovskite. Mg-perovskite is formed only by the majorite-perovskite transition.

3.3. Partitioning of Aluminum and Stabilities of Majorite and Mg-perovskite

[21] The stabilities of akimotoite, majorite, and Mg-perovskite have been precisely determined on the join $MgSiO_3$-$Mg_3Al_2Si_3O_{12}$ [*Irifune et al.*, 1996; *Kubo and Akaogi*, 2000; *Hirose et al.*, 2001a]. The Al_2O_3 contents in coexisting phases make the two-phase loop (Figure 5). The stabilities and relative proportions of akimotoite, majorite, and perovskite in the simplified pyrolite-like composition in SiO_2-MgO-Al_2O_3 (3:2 mixture of Mg_2SiO_4 and $MgSiO_3$ plus 10% Al_2O_3 in weight) are illustrated (Figure 5). It is noted that the average Al_2O_3 content in these Al-bearing phases, shown by the arrows, significantly decreases from 10 to 4.8% upon decomposition of ringwoodite or wadslyite. At 1750°C, perovskite is formed by the univariant reaction of akimotoite-perovskite transition, and its proportion suddenly increases by the decomposition of ringwoodite. Majorite then disappears at slightly higher pressures within 0.8 GPa. The maximum solubility of Al_2O_3 in perovskite defines the complete transformation from majorite to perovskite. At 2000°C, perovskite is formed by the decomposition of wadslyite. Even at higher pressures, majorite is stable in a wide pressure range of 2.4 GPa.

[22] The stabilities of akimotoite, majorite, and Mg-perovskite in the natural pyrolite composition are very similar to those in the simplified system described above. The Al contents in coexisting akimotoite, majorite, and Mg-perovskite were similarly plotted in Figure 6. Akimotoite and majorite or majorite and Mg-perovskite form two-phase loop. The phase stabilities and relative proportions of these Al-bearing $MgSiO_3$-rich phases are shown in Figure 6. A minor amount of Al_2O_3 partitioned into trace Ca-perovskite was neglected in Figure 6. The arrows indicate the average Al_2O_3 content over the $MgSiO_3$-rich phases present, which is significantly diluted by the postspinel phase transition. At 1600°C, Mg-perovskite is formed by the nearly univariant reaction of the akimotoite-perovskite transition. Its proportion suddenly increases upon decomposition of ringwoodite, and majorite disappears during decomposition. At 1800°C it is shown that the postspinel phase and majorite-perovskite transitions occur at similar pressures. At 2000°C, Mg-perovskite is formed when a majority of ringwoodite decomposes. Even at higher pressures, majorite is stable in a wide pressure range of 1 GPa. Majorite garnet disappears below 24.1 GPa at 1600–2000°C. Note that Al contents in majorite coexisting with perovskite significantly decrease with increasing temperature, while those in perovskite change little with temperature (Figure 6d). Mg-perovskite-in curve above 1600°C has a higher dP/dT slope (more temperature-dependent) than majorite-out curve in Figure 4, since they are controlled by the minimum solubility of Al in majorite and the maximum solubility of Al in Mg-perovskite, respectively.

3.4. Mineral Proportions

[23] The volume fractions of minerals found in the pyrolitic mantle composition were calculated from the density and the weight fraction of each constituent mineral. The density at high pressure and high temperature was calculated using the chemical composition and the thermoelastic parameters, according to the method of *Weidner and Wang* [1998]. Only the parameters of akimotoite were taken from *Wang et al.* [2000]. The weight fraction was obtained by the mass balance calculation using chemical composition of each phase. For the experiments the composition of Ca-perovskite or magnesiowüstite was not obtained; that analyzed in the run C188 or C132, respectively, was used. This should not change the results significantly because their compositions were similar between the experiments. For the run C186 including more than four phases, the proportion of ringwoodite was determined by compositional mapping with the microprobe. A trace amount of stishovite found in the run C190 was neglected. The results are shown in Figure 7 for each temperature.

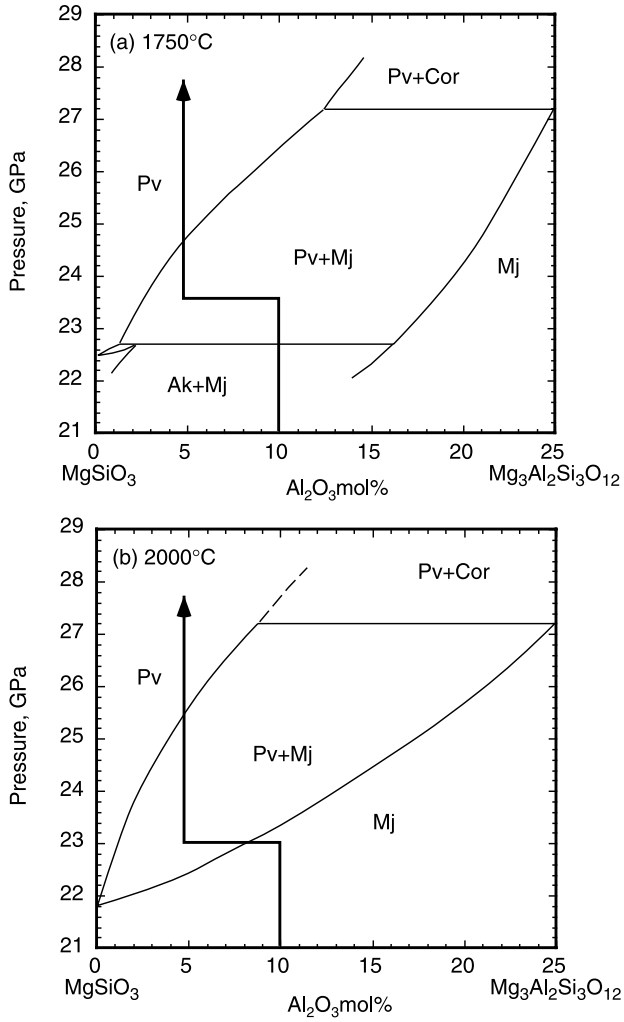

Figure 5. Phase relations on the join $MgSiO_3$-$Mg_3Al_2Si_3O_{12}$ (modified from *Hirose et al.* [2001a] on the basis of Jamieson et al.'s gold pressure scale). The stabilities and relative proportions of majorite and perovskite in the simplified pyrolite-like composition in SiO_2-MgO-Al_2O_3 are illustrated using the arrow, indicating the average Al_2O_3 content in $MgSiO_3$-rich phases present (akimotoite, majorite, or Mg-perovskite). See the text for details. Majorite is stable in a wide pressure range at higher pressures than the postspinel phase boundary at 2000°C.

4. Buoyancy of Plumes at the 670-km Boundary

[24] Figure 8 shows the bulk density profiles of the pyrolite composition as a function of depth. They were calculated on the basis of the mineral proportions shown in Figure 7. The calculation showed that density decreases with increasing depth at 635–645 km along the 2000°C isotherm, corresponding to the ringwoodite to majorite and magnesiowüstite transition. However,

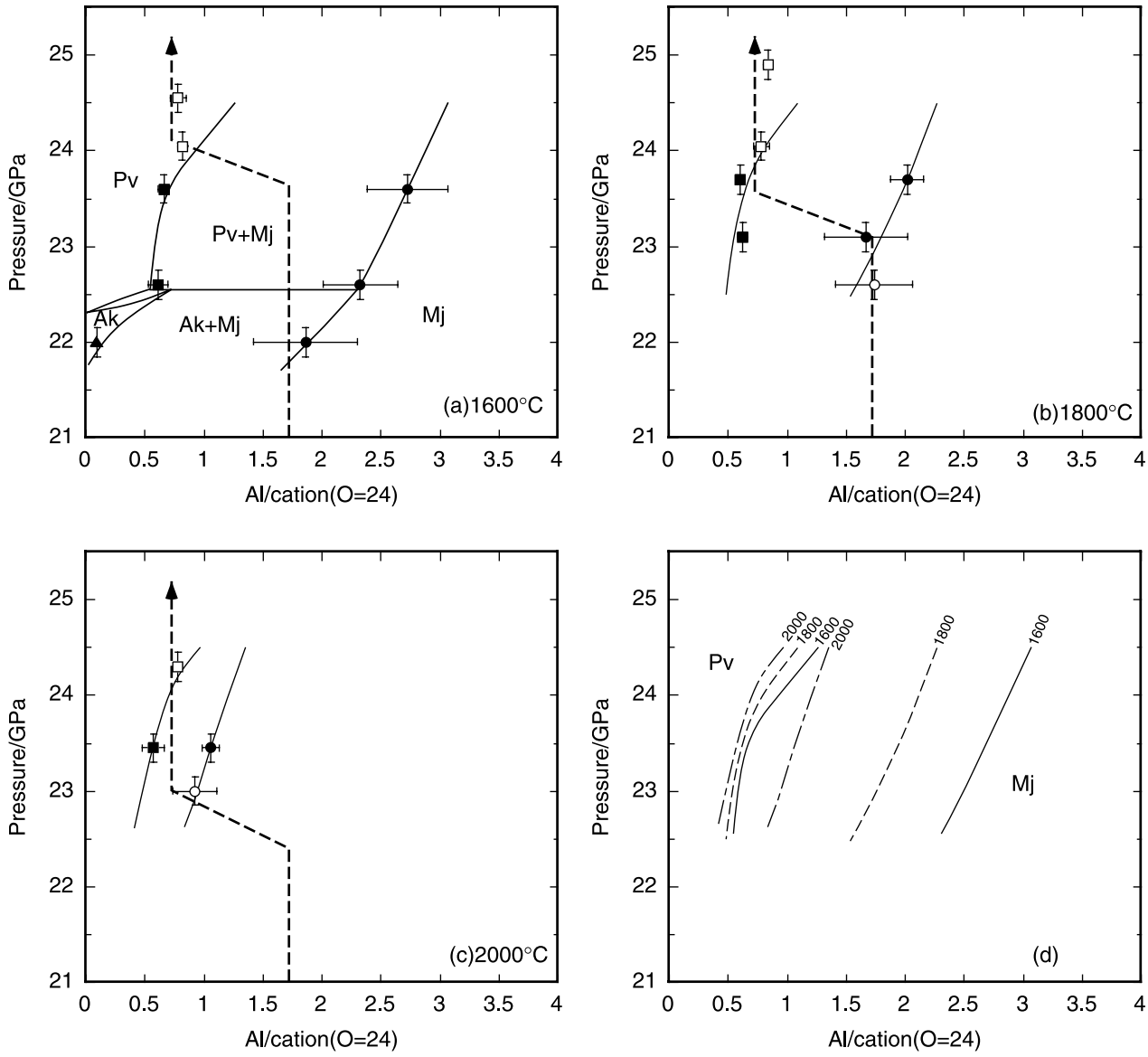

Figure 6. Al contents in akimotoite, majorite, and Mg-perovskite synthesized in the pyrolitic mantle composition. (a–c) The coexisting assemblages are shown by the solid symbols. The stabilities and relative proportions of akimotoite, majorite, and Mg-perovskite are illustrated using the arrow, indicating the average Al content in these phases. See the text for details. (d) Majorite-perovskite two-phase loops are shown at 1600, 1800, and 2000°C. Note that Al contents in majorite coexisting with perovskite significantly decrease with increasing temperature, while those in perovskite change little with temperature.

it must be due to the uncertainty of thermoelastic parameters of these minerals.

[25] Along the isotherm at 1600°C, density jumps are recognized both around 640-km and 670-km depth. The 0.7% density jump at 638-km depth is caused by the akimotoite-perovskite transition. The latter is caused by the postspinel phase transitions, and the depth coincides with that in the preliminary Earth reference model (PREM) [*Dziewonski and Anderson*, 1981]. The 8.1% density increase is also comparable to that in the PREM (9.7%).

[26] The 670-km boundary has long been believed to be a barrier for mantle convection, impeding subduction of slabs or upwelling of hot plumes, because perovskite, the dense lower mantle mineral, has been believed to be formed simply by the postspinel phase transition with a negative Clausius-Clapeyron slope. The present study, however, demonstrates that the formation of Mg-rich perovskite occurs by various reactions, not only the postspinel phase transition but also the akimotoite-perovskite and/or majorite-perovskite transitions. It is noted that Mg-perovskite-in curve shown in Figure 4 is primarily controlled by the akimotoite-perovskite or majorite-perovskite transitions. The contours of volume fraction of Mg-perovskite have temperature-independent or positive pressure-temperature slopes above 1700–1800°C (Figure 4b), indicating that the formation of Mg-perovskite occurs by a positive Clapeyron slope above this temperature.

[27] Plumes originating from the Earth's lower mantle may have temperatures higher than 1800°C at 670-km depth, which is higher by 200–300°C than the global average [e.g., *Watson and McKenzie*, 1991; *Ribe and Christensen*, 1999; *Li et al.*, 2000]. Within such high-temperature plumes, a majority of Mg-perovskite transforms to majorite, and then ringwoodite is formed from majorite and magnesiowüstite at shallower depths (Figure 4). It is noted that the former transition from perovskite-dominant to majorite-dominant

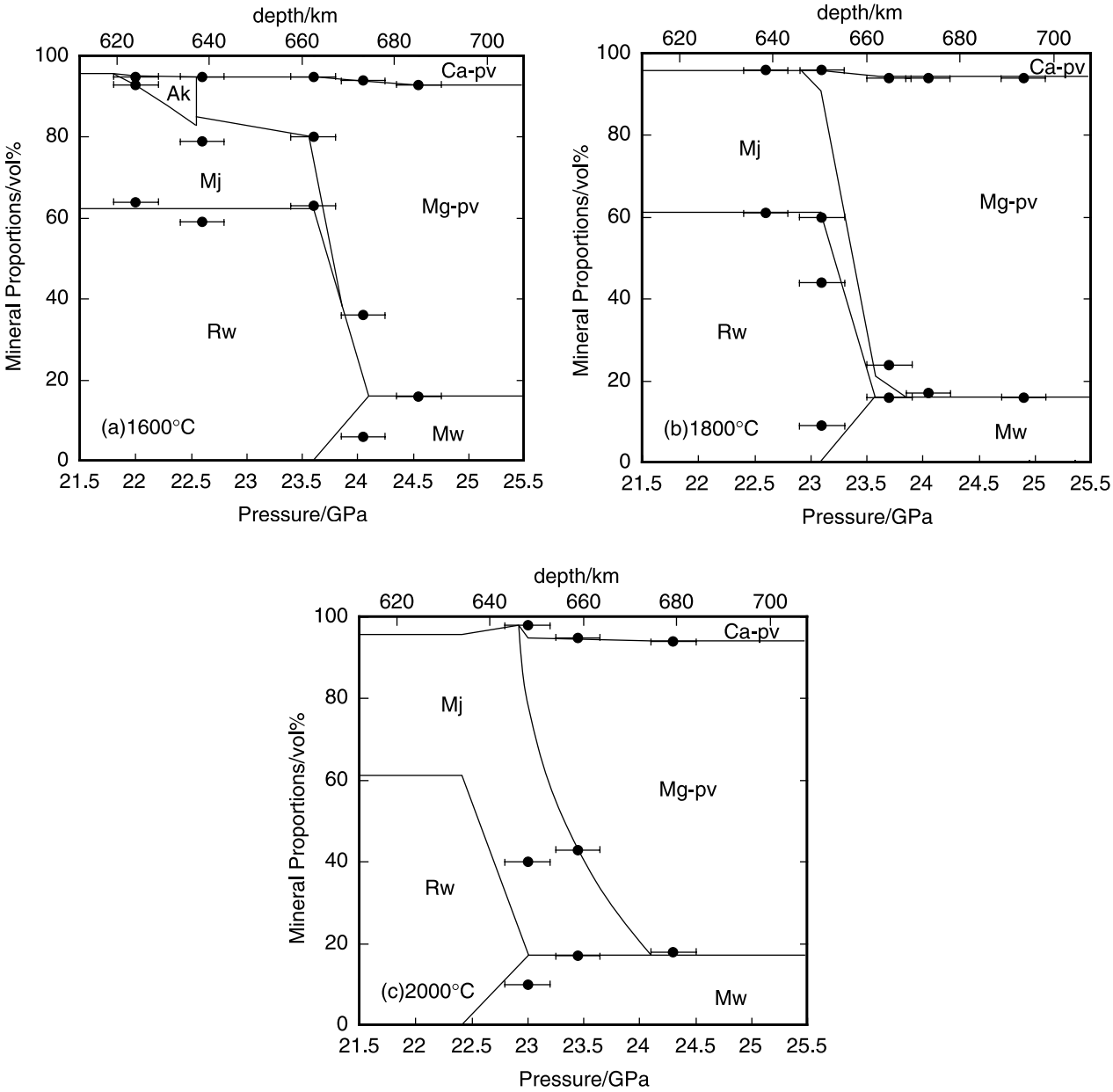

Figure 7. Mineral proportions (vol %) in the pyrolitic mantle composition. Phase boundaries are referred from Figure 4.

mineral assemblage causes a large density drop (~9%), but the latter one from majorite-dominant to ringwoodite-dominant assemblage makes a minimal change in density. Such phase transitions within plumes facilitate their ascent to the mantle transition zone through the 670-km boundary because the phase transition from perovskite to majorite has a positive Clausius-Clapeyron slope. The further transition to a ringwoodite-dominant assemblage does not cause the buoyancy effect in the dynamics, although it has a negative Clapeyron slope.

[28] As shown in Figure 8, the density crossover is largely observed between profiles of 1600 and 1800°C in a depth interval from 653 to 674 km. It is noted, however, that the crossover significantly reduces at higher temperatures. The density crossover between those at 1800 and 2000°C is quite limited, both in the depth interval and the magnitude. The 2000°C portion within the plume is buoyant at most of the depth range during phase transitions and synthetically has a positive buoyancy compared to the 1800°C portion around the 670-km boundary. Thus the 670-km boundary works as an accelerator rather than a barrier for the high-temperature plumes upwelling from the lower mantle.

[29] The buoyancy induced by phase transitions around 670-km depth is strongly dependent on temperature. It resists convection in a cold region such as subduction zone, where the formation of Mg-perovskite is dominated by the postspinel and the akimotoite-perovskite phase transitions, both of which have negative Clausius-Clapeyron slopes. On the other hand, it assists convection in a hot region, where Mg-perovskite transforms to majorite by the majorite-perovskite transition with a positive Clapeyron slope. The 670-km discontinuity works like a thermostat that may have kept the temperature of the mantle rather constant through the history of the Earth [*Weidner and Wang*, 1998]. It primarily resists convection at present except beneath some hot spots, and the limited amount of heat and material is currently being transferred from the lower mantle. It may result in a temperature increase of the lower

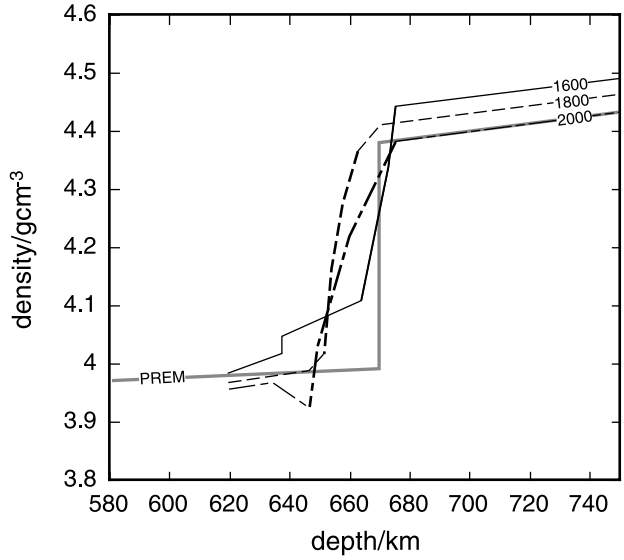

Figure 8. Calculated density profiles of the pyrolitic mantle composition along 1600, 1800, and 2000°C isotherms. The curve of preliminary Earth reference model (PREM) is shown for comparison [*Dziewonski and Anderson*, 1981].

mantle and a decrease of the upper mantle temperature mainly due to magma generation near the surface. However, when the temperature of the lower mantle becomes high enough (>1800°C), a large amount of heat and material may be introduced through the boundary. There may have been a pulse in the oceanic crust production rate at 100–120 Ma in both ridges and plateaus (mid-Cretaceous superplume) [*Larson*, 1991], although it is still in debate [e.g., *Heller et al.*, 1996]. Also, the continents are likely to have grown episodically since the Archean [*Condie*, 1998; *McCulloch and Bennett*, 1994]. These may reflect a large input of heat from the lower mantle and a rejuvenation of the upper mantle.

5. Depth of the 670-km Discontinuity Beneath Hot Spot

[30] The depth of the 670-km discontinuity has been used to estimate temperatures at that depth. Simply assuming that the seismic discontinuity is caused only by the postspinel phase transition, the elevation of the 670-km boundary depth is expected in a hot region. However, this study shows that this assumption does not stand above 1800°C if the transition zone has a pyrolitic composition. The depth of the 670-km seismic discontinuity is less temperature-dependent and is slightly deeper with increasing temperature above 1800°C (Figure 8).

[31] The recent seismic observations at South Pacific superswell and Iceland showed the normal to slightly depressed 670-km and the deeper 410-km discontinuities [*Vinnik et al.*, 1997; *Shen et al.*, 1998]. If the deeper 410-km discontinuity indicates the presence of high-temperature anomaly, the slightly depressed 670-km discontinuity could suggest that the temperatures beneath these hot spots could exceed 1800°C at 670-km depth. On the other hand, the depth of 670-km discontinuity is uplifted at Hawaii and Yellowstone [*Li et al.*, 2000; *Humphreys et al.*, 2000]. The temperatures of plumes forming these hot spots may be lower than those at South Pacific and Iceland.

[32] The excess temperature was estimated to be >150°C beneath Iceland from the thickness of the transition zone [*Shen et al.*, 1998]. It is even less by ~100°C than that suggested for Hawaiian plume similarly from the transition zone thickness [*Li et al.*, 2000]. In these studies it was simply assumed that the transition zone is thinner at higher temperature due to the deeper 410-km and the shallower 670-km discontinuities. The thin transition zone, however, can be attributed only to the deep 410-km discontinuity for Iceland, since the 670-km discontinuity is not uplifted. This value is therefore likely to be underestimate, and the larger excess temperatures may be necessary to explain the observed thin transition zone beneath Iceland.

[33] The present study also suggests that the broad velocity discontinuity is expected at the 670-km boundary in a hot region. The majorite-perovskite phase transition is responsible for the large velocity increase at this depth in a high-temperature region, which occurs in a wider depth interval than the postspinel phase transition. The density profile in Figure 8 shows that the broad density jump occurs in a depth range from 646 to 675 km along the 2000°C isotherm. The broad 670-km discontinuity has been observed beneath the South Pacific superswell [*Vinnik et al.*, 1997]. It likely reflects the large velocity change caused by the majorite-perovskite phase transition in a relatively wide depth range rather than the presence of hot material below 670-km boundary (stagnant plume) as argued by *Vinnik et al.* [1997].

[34] **Acknowledgments.** The author thanks S. Maruyama, E. Takahashi, and S. Kaneshima for discussions and constructive comments. Y. Nishihara is acknowledged for the technical advice. The gel starting material was provided from T. Kawamoto. The author thanks H. Green, C. Herzberg, and an anonymous referee for reviews.

References

Akaogi, M., and E. Ito, Refinement of enthalpy measurement of $MgSiO_3$ perovskite and negative pressure-temperature slopes for perovskite-forming reactions, *Geophys. Res. Lett.*, *20*, 1839–1842, 1993.

Anderson, O. L., D. G. Isaak, and S. Yamamoto, Anharmonicity and the equation of state for gold, *J. Appl. Phys.*, *65*, 1534–1543, 1989.

Bertka, C. M., and Y. Fei, Mineralogy of Martian interior up to core-mantle boundary pressures, *J. Geophys. Res.*, *102*, 5251–5264, 1997.

Chudinovskikh, L., and R. Boehler, High-pressure polymorphs of olivine and the 660-km seismic discontinuity, *Nature*, *411*, 574–577, 2001.

Condie, K. C., Episodic continental growth and supercontinents: A mantle avalanche connection?, *Earth Planet. Sci. Lett.*, *163*, 97–108, 1998.

Dziewonski, A. M., and D. L. Anderson, Preliminary reference Earth model, *Phys. Earth Planet. Inter.*, *25*, 297–356, 1981.

Fukao, Y., M. Obayashi, H. Inoue, and M. Nenbai, Subducting slabs stagnant in the mantle transition zone, *J. Geophys. Res.*, *97*, 4809–4822, 1992.

Heller, P. L., D. L. Anderson, and C. L. Angevine, Is the middle Cretaceous pulse of rapid sea-floor spreading real or necessary?, *Geology*, *24*, 491–494, 1996.

Herzberg, C., P. Raterron, and J. Zhang, New experimental observations on the anhydrous solidus for peridotite KLB-1, *Geochem. Geophys. Geosyst., 1*, Paper 2000GC000089, 2000.

Hirose, K., and I. Kushiro, Partial melting of dry peridotites at high pressures: Determination of compositions of melts segregated from peridotite using aggregates of diamond, *Earth Planet. Sci. Lett.*, *114*, 477–489, 1993.

Hirose, K., Y. Fei, Y. Ma, and H. K. Mao, The fate of subducted basaltic crust in the Earth's lower mantle, *Nature*, *397*, 53–56, 1999.

Hirose, K., Y. Fei, S. Ono, T. Yagi, and K. Funakoshi, In situ measurements of the phase transition boundary in $Mg_3Al_2Si_3O_{12}$: Implications for the nature of the seismic discontinuities in the Earth's mantle, *Earth Planet. Sci. Lett.*, *184*, 567–573, 2001a.

Hirose, K., T. Komabayashi, M. Murakami, and K. Funakoshi, In situ measurements of the majorite-akimotoite-perovskite phase transition boundaries in $MgSiO_3$, *Geophys. Res. Lett.*, *28*, 4351–4354, 2001b.

Humphreys, E. D., K. G. Dueker, D. L. Schutt, and R. B. Smith, Beneath Yellowstone: Evaluating plume and nonplume models using teleseismic images of the upper mantle, *GSA Today*, *10*(12), 1–7, 2000.

Irifune, T., Absence of an aluminous phase in the upper part of the lower mantle, *Nature*, *370*, 131–133, 1994.

Irifune, T., T. Koizumi, and J. Ando, An experimental study of the garnet-perovskite transformation in the system $MgSiO_3$-$Mg_3Al_2Si_3O_{12}$, *Phys. Earth Planet. Inter.*, *69*, 147–157, 1996.

Irifune, T., et al., The postspinel phase boundary in Mg_2SiO_4 determined by in situ X-ray diffraction, *Science*, *279*, 1698–1700, 1998.

Ito, E., and E. Takahashi, Postspinel transformations in the system Mg_2SiO_4-Fe_2SiO_4 and some geophysical implications, *J. Geophys. Res.*, *94*, 10,637–10,646, 1989.

Jamieson, J. C., J. N. Fritz, and M. H. Manghnani, Pressure measurement at high temperature in x-ray diffraction studies: Gold as a primary standard, in *High-Pressure Research in Geophysics*, edited by S. Akimoto and M. H. Manghnani, pp. 27–48, Cent. for Acad. Publ. Jpn., Tokyo, 1982.

Kawamoto, T., and J. R. Holloway, Melting temperature and partial melt chemistry of H_2O-saturated mantle peridotite to 11 gigapascals, *Science*, *276*, 240–243, 1997.

Kubo, A., and M. Akaogi, Post-garnet transitions in the system $Mg_4Si_4O_{12}$-$Mg_3Al_2Si_3O_{12}$ up to 28 GPa: Phase relations of garnet, ilmenite and perovskite, *Phys. Earth Planet. Inter.*, *121*, 85–102, 2000.

Kuroda, K., T. Irifune, T. Inoue, N. Nishiyama, M. Miyashita, K. Funakoshi, and W. Utsumi, Determination of the phase boundary between ilmenite and perovskite in $MgSiO_3$ by in situ X-ray diffraction and quench experiments, *Phys. Chem. Mineral.*, *27*, 523–532, 2000.

Larson, R. L., Latest pulse of Earth: Evidence for a mid-Cretaceous superplume, *Geology*, *19*, 547–550, 1991.

Li, X., R. Kind, K. Priestley, S. V. Sobolev, F. Tajima, X. Yuan, and M. Weber, Mapping the Hawaiian plume conduit with converted seismic waves, *Nature*, *405*, 938–941, 2000.

McCulloch, M. T., and V. C. Bennett, Progressive growth of the Earth's continental crust and depleted mantle: Geochemical constraints, *Geochem. Cosmochim. Acta*, *58*, 4717–4738, 1994.

Ono, S., and A. Yasuda, Compositional change of majoritic garnet in a MORB composition from 7 to 17 GPa and 1400 to 1600°C, *Phys. Earth Planet. Inter.*, *96*, 171–179, 1996.

Ono, S., T. Katsura, E. Ito, M. Kanzaki, A. Yoneda, M. J. Walter, S. Urakawa, W. Utsumi, and K. Funakoshi, In situ observation of ilmenite-perovskite phase transition in $MgSiO_3$ using synchrotron radiation, *Geophys. Res. Lett.*, *28*, 835–838, 2001.

Ribe, N. M., and U. R. Christensen, The dynamical origin of Hawaiian volcanism, *Earth Planet. Sci. Lett.*, *171*, 517–531, 1999.

Sawamoto, H., Phase diagram of $MgSiO_3$ at pressures up to 24 GPa and temperatures up to 2200 K: Phase stability and properties of tetragonal garnet, in *High Pressure Research in Mineral Physics, Geophys. Monogr. Ser.*, vol 39, edited by M. H. Manghnani and Y. Syono, pp. 209–219, AGU, Washington, D. C., 1987.

Shen, Y., S. C. Solomon, I. T. Bjarnason, and C. J. Wolfe, Seismic evidence for a lower-mantle origin of the Iceland plume, *Nature*, *395*, 62–65, 1998.

Shim, S.-H., T. S. Duffy, and G. Shen, Evidence that the post-spinel transformation in Mg_2SiO_4 is responsible for the 660-km seismic discontinuity, *Nature*, *411*, 571–574, 2001.

Takahashi, E., Melting of dry peridotite KLB-1 up to 14 GPa: Implication for the origin of peridotitic upper mantle, *J. Geophys. Res.*, *91*, 9367–9382, 1986.

Van der Hilst, R., R. Engdahl, W. Spackman, and G. Nolet, Tomographic imaging of subducted lithosphere below northwest Pacific island arcs, *Nature*, *353*, 37–43, 1991.

Vinnik, L., S. Chevrot, and J. P. Montagner, Evidence for stagnant plume in the transition zone?, *Geophys. Res. Lett.*, *24*, 1007–1010, 1997.

Wang, Y., T. Uchida, D. Weidner, J. Zhang, M. Rivers, and S. Sutton, Thermal equation of state of $MgSiO_3$ ilmenite and mineral physics constraints on the transition zone structure, *Eos Trans. AGU*, *81*, West Pac. Geophys. Meet. Suppl., Abstract T31A-09, 2000.

Watson, S., and D. McKenzie, Melt generation by plumes: A study of Hawaiian volcanism, *J. Petrol.*, *32*, 501–537, 1991.

Weidner, D., and Y. Wang, Chemical- and Clapeyron-induced buoyancy at the 660 km discontinuity, *J. Geophys. Res.*, *103*, 7431–7441, 1998.

Wood, B. J., Phase transformations and partitioning relations in peridotite under lower mantle conditions, *Earth Planet. Sci. Lett.*, *174*, 341–354, 2000.

Zhang, J., and C. Herzberg, Melting experiments on anhydrous peridotite KLB-1 from 5.0 to 22.5 GPa, *J. Geophys. Res.*, *99*, 17,729–17,742, 1994.

K. Hirose, Department of Earth and Planetary Sciences, Tokyo Institute of Technology, 2-12-1 Ookayama, Meguro, Tokyo 152-8551, Japan. (kei@geo.titech.ac.jp)